PNAS RESEARCH ARTICLE | BIOCHEMISTRY OPEN ACCESS

Human transferrin receptor can mediate SARS-CoV-2 infection

Zhiyi Liao[a,b,1], Chaoming Wang[a,b,1], Xiaopeng Tang[a,c,1], Mengli Yang[d,1], Zilei Duan[a,1], Lei Liu[e,1], Shuaiyao Lu[d,1], Lei Ma[d,1], Ruomei Cheng[a], Gan Wang[a], Hongqi Liu[d], Shuo Yang[a,b], Jingwen Xu[d], Dawit Adisu Tadese[a,b], James Mwangi[a,b], Peter Muiruri Kamau[a,b], Zhiye Zhang[a], Lian Yang[f], Guoyang Liao[d,2], Xudong Zhao[e,2], Xiaozhong Peng[d,2], and Ren Lai[a,2]

Edited by Stanley Perlman, The University of Iowa, Iowa City, IA; received October 9, 2023; accepted January 8, 2024 by Editorial Board Member Bernard Moss

Severe acute respiratory syndrome coronavirus 2 (SARS-CoV-2) infection has been detected in almost all organs of coronavirus disease-19 patients, although some organs do not express angiotensin-converting enzyme-2 (ACE2), a known receptor of SARS-CoV-2, implying the presence of alternative receptors and/or co-receptors. Here, we show that the ubiquitously distributed human transferrin receptor (TfR), which binds to diferric transferrin to traffic between membrane and endosome for the iron delivery cycle, can ACE2-independently mediate SARS-CoV-2 infection. Human, not mouse TfR, interacts with Spike protein with a high affinity (K_D ~2.95 nM) to mediate SARS-CoV-2 endocytosis. TfR knock-down (TfR-deficiency is lethal) and overexpression inhibit and promote SARS-CoV-2 infection, respectively. Humanized TfR expression enables SARS-CoV-2 infection in baby hamster kidney cells and C57 mice, which are known to be insusceptible to the virus infection. Soluble TfR, Tf, designed peptides blocking TfR-Spike interaction and anti-TfR antibody show significant anti-COVID-19 effects in cell and monkey models. Collectively, this report indicates that TfR is a receptor/co-receptor of SARS-CoV-2 mediating SARS-CoV-2 entry and infectivity by likely using the TfR trafficking pathway.

SARS-CoV-2 | alternative receptors | transferrin receptor | spike | interaction

Significance

SARS-CoV-2 has been detected in almost all organs of COVID-19 patients, although some of the organs express little or no ACE2. Single-cell sequencing indicates that SARS-CoV-2 is present in diverse immune cells, which do not express ACE2, suggesting the presence of other receptors/co-receptors mediating virus entry. Here, we identified human TfR, one of the most ubiquitously and highly expressed membrane components, as a receptor of SARS-CoV-2. TfR mediated SARS-CoV-2 infection by directly binding to the spike with high affinity and transporting the virus into the host cells. Interference with the TfR and SARS-CoV-2 interaction significantly inhibited viral infection. This study indicates that TfR is an alternative target for SARS-CoV-2 infection. The TfR trafficking pathway mediates SARS-CoV-2 entry and infectivity.

Severe acute respiratory syndrome coronavirus 2 (SARS-CoV-2), declared a pandemic by the World Health Organization (WHO) on 11 March 2020 (https://www.who.int/), is the cause of COVID-19. This disease is characterized by influenza-like manifestations ranging from mild to severe pneumonia, fatal acute lung injury, acute respiratory distress syndrome, multi-organ failure, and relatively high morbidity and mortality, especially in older patients with comorbidities (1–10). Unfortunately, the pathogenesis and etiology of COVID-19 are yet to be clarified, and targeted therapies for COVID-19 patients remain inadequate (11).

Pioneering studies (12, 13) demonstrated that angiotensin-converting enzyme 2 (ACE2) is the critical receptor for SARS-CoV, which first emerged 20 y ago (14). The spike protein of SARS-CoV binds to the host ACE2 receptor and then enters target cells. SARS-CoV-2 bears an 82% resemblance to the genomic sequence of SARS-CoV (15). The spike receptor-binding domain (RBD) of SARS-CoV-2 is also highly similar to that of SARS-CoV, suggesting a possible common host cell receptor. Several cryoelectron microscopy studies have demonstrated that SARS-CoV-2 spike protein directly binds to ACE2 with high affinity (16–20). Soluble ACE2 fused to Ig (18) or nonspecific protease inhibitors (e.g., camostat mesylate) can hinder infection with a pseudovirus-bearing the SARS-CoV-2 spike protein (21). Camostat mesylate at high doses (100 mg/mL) can also partially reduce SARS-CoV-2 growth (21). Recently, Monteil et al. reported that clinical-grade soluble human ACE2 can significantly block the early stages of SARS-CoV-2 infection in engineered human tissues (19). SARS-CoV-2 preferentially infects cells of the respiratory tract (22). The virus has been detected in almost all human organs, although some express little or no ACE2 (23–25). Single-cell sequencing data indicate that SARS-CoV-2 RNAs are present in diverse immune cells that do not express ACE2, suggesting the possibility of other receptors/co-receptors mediating virus entry (26–29). Indeed, recent research has shown that neuropilin-1 facilitates SARS-CoV-2 cell entry and infectivity (30). Tyrosine-protein kinase receptors UFO (AXL), CD4, CD147, KREMEN, HSPGs, sialic acids, TMEM106B, and NPC1 have also been suggested as alternative receptors for SARS-CoV-2 (31–38). LRRC15 was reported as an inhibitory receptor for SARS-CoV-2 entry (39).

Here, we identified the transferrin receptor (TfR) as another receptor that mediates SARS-CoV-2 entry by directly binding to the virus spike protein with high affinity. Notably, interference with the spike-TfR interactions by small peptides and antibodies significantly inhibited SARS-CoV-2 infection in cells and monkeys. This provides a potential antiviral

Author contributions: Z.L., C.W., X.T., and R.L. designed research; Z.L., C.W., X.T., M.Y., Z.D., L.L., S.L., L.M., R.C., S.Y., J.X., and Z.Z. performed research; G.W., H.L., and L.Y. contributed new reagents/analytic tools; Z.L., C.W., X.T., G.L., X.Z., X.P., and R.L. analyzed data; and Z.L., C.W., X.T., D.A.T., J.M., P.M.K., and R.L. wrote the paper.

The authors declare no competing interest.

This article is a PNAS Direct Submission. S.P. is a guest editor invited by the Editorial Board.

[1]Z.L., C.W., X.T., M.Y., Z.D., L.L., S.L., and L.M. contributed equally to this work.

[2]To whom correspondence may be addressed. Email: liaogy@imbcams.com.cn, zhaoxudong@wchscu.cn, pengxiaozhong@pumc.edu.cn, or rlai@mail.kiz.ac.cn.

This article contains supporting information online at https://www.pnas.org/lookup/suppl/doi:10.1073/pnas.2317026121/-/DCSupplemental.

Published February 26, 2024.

strategy and an animal model of mice expressing humanized TfR (hTfR) to study viral infections and drug screening.

Results

TfR Is Highly Expressed in the Lungs and Is Up-Regulated upon SARS-CoV-2 Infection. To identify host proteins responsible for SARS-CoV-2 infection of pulmonary cells, we explored the proteins that interacted with spike in human lung adenocarcinoma (Calu-3) cells by co-immunoprecipitation (Co-IP) and liquid chromatography–tandem mass spectrometry (LC–MS/MS). In total, we identified 293 proteins that interacted with spike, 42 of which were transmembrane proteins, 9 of which were cell membrane proteins or were able to translocate to the cell membrane, and 2 (transferrin receptor protein 1, TfR, angiotensin-converting enzyme 2, ACE2) of which were reported to be associated with viral entry (*SI Appendix*, Fig. S1) (40). Many viruses via TfR, which is the primary gatekeeper of iron metabolism, to enter cells (41–43). Furthermore, TfR is ubiquitously and highly expressed in plasma membranes (41). As such, we investigated and compared the TfR expression in the liver and respiratory tract organs (i.e., nasal cavity, trachea, and lungs) of mice. At both the RNA (Fig. 1*A*) and protein levels (Fig. 1*B*), TfR expression was much higher in the trachea and lungs than in other tissues of mice. We further analyzed the effects of SARS-CoV-2 infection on the expression of TfR in the lung tissues of monkeys and humanized ACE2 (hACE2) mice (Fig. 1 *C* and *D*) using immunohistochemical (IHC) analysis. We also stained for viral antigens to determine the extent of virus infection (Fig. 1 *E* and *F*). Results showed that TfR expression increased 1.8- and 1.5-fold upon SARS-CoV-2 infection in the lungs of the monkeys and mice, respectively.

Human TfR Directly Interacts with SARS-CoV-2 Spike Protein. As TfR is a multi-tasking receptor that mediates cell entry of many different viruses (41) and as SARS-CoV-2 appears to up-regulate TfR expression (as shown above), we investigated whether TfR directly interacts with SARS-CoV-2. Enzyme-linked immunosorbent assay (ELISA) and surface plasmon resonance (SPR) analysis indicated a direct interaction between human TfR and the SARS-CoV-2 spike protein (Fig. 2 *A* and *B* and *SI Appendix*, Fig. S2 *A* and *B*). The association rate constant (Ka), dissociation rate constant (Kd), and equilibrium dissociation constant (K_D) for the TfR and spike protein interactions were 2.69×10^5 M^{-1} s^{-1}, 7.92×10^{-4} s^{-1}, and 2.95 nM, respectively. Interactions between TfR and SARS-CoV-2 spike RBD, which binds to the cell receptor ACE2 (44, 45), were also investigated using SPR (Fig. 2*C* and *SI Appendix*, Fig. S2*C*). The K_D value between TfR and SARS-CoV-2 spike RBD was ~43 nM, which is slightly weaker than the binding affinity between TfR and intact spike protein. Importantly, SARS-CoV-2 spike protein shows no interaction with mouse and Syrian hamster TfR (*SI Appendix*, Fig. S3). Based on the TfR (46) and virus spike protein structures (47), we established a TfR-spike protein interaction docking model (*SI Appendix*, Fig. S4*A*). According to the model, two peptides derived from TfR sequence (SL8: SKVEKLTL and QK8: QDSNWASK), which were predicted to interfere with the interface mediating TfR-spike protein interaction (*SI Appendix*, Table S1). As illustrated in Fig. 2*D*, the peptides inhibited TfR-spike protein

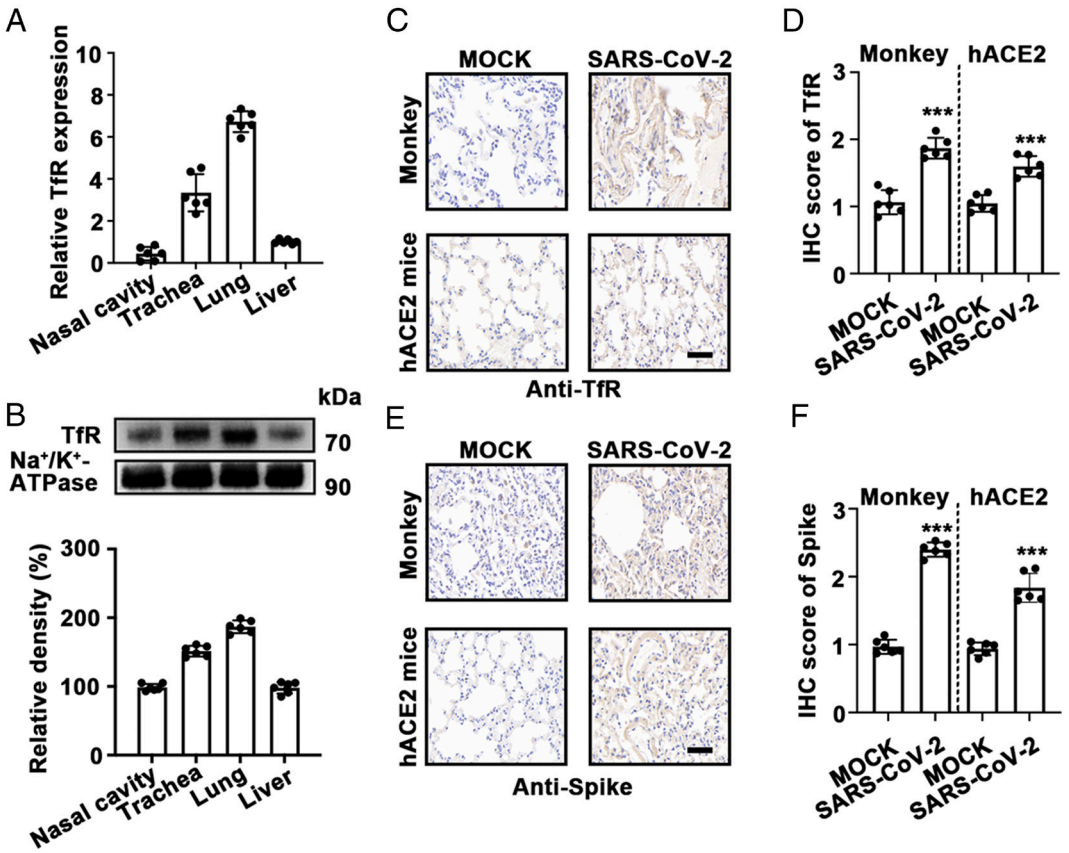

Fig. 1. TfR is highly expressed in lungs and up-regulated upon SARS-CoV-2 infection. TfR expression levels in different tissues, including respiratory tract (nasal cavity, trachea, and lung) and liver of C57 mice, were detected by qRT-PCR (*A*) and western blotting (*B*). Fold change was in comparison to "liver". Na^+/K^+ ATPase was used as a control. Data represent mean ± SD of six independent experiments. IHC analysis of TfR expression and viral antigen (*C*–*F*) in lung tissue of SARS-CoV-2-infected monkeys and hACE2 mice. The cells stained brown are positive for TfR or viral antigen. Cell nuclei are stained blue with hematoxylin. (Scale bar, 50 μm.) Data represent mean ± SD (n = 6), ***$P < 0.001$ by the unpaired *t* test.

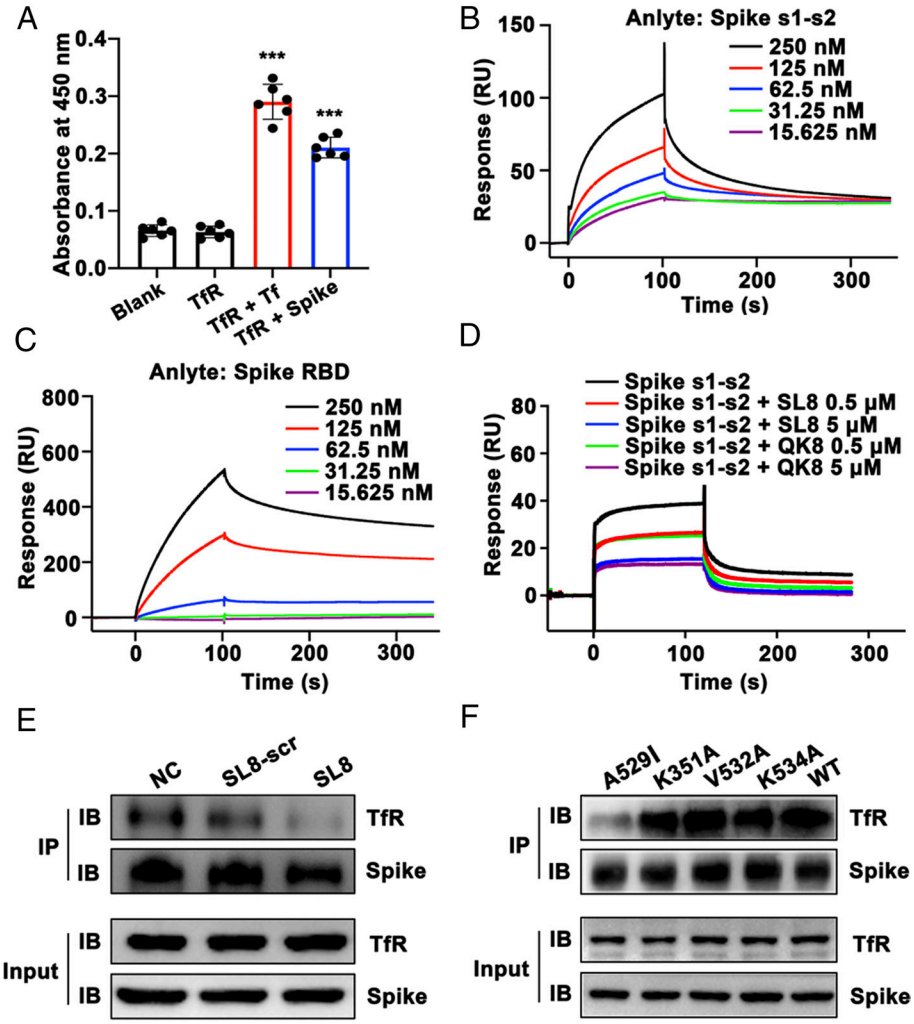

Fig. 2. Direct interaction between spike and human TfR. (*A*) Interaction between spike protein and TfR was analyzed by ELISA. Data represent mean ± SD of six independent experiments, ***$P < 0.001$ by the unpaired *t* test. (*B*) SPR analysis of TfR-spike s1-s2 protein interaction. (*C*) SPR analysis of the interaction between TfR and spike protein receptor-binding domain (RBD). (*D*) Effects of inhibitory peptides (SL8 and QK8) on TfR-spike protein interaction were analyzed by SPR. (*E*) Effects of SL8 and its scrambled peptide (SL8-scr) on TfR-spike protein complex formation were analyzed by Co-IP. (*F*) TfR mutants (A529I, K531A, V532A, and K534A; 2 μg) were incubated with wild-type spike (2 μg), anti-spike antibody (5 μg), and protein A agarose (20 μL) overnight. Binding was measured by Co-IP. Images are representative of at least three independent experiments. IP: immunoprecipitation; IB: immunoblotting.

interactions by SPR analysis. Co-IP analysis also revealed that SL8, but not its scrambled peptide (SL8-scr), interfered with TfR-spike protein complex formation (Fig. 2*E*), suggesting that the key region mediating TfR-spike protein interaction is located on αIII-2 (524–537) of the helical domain on TfR. Based on the docking model in *SI Appendix*, Fig. S4*A*, four TfR residues (A529, K531, V532, and K534) were predicted to be important for TfR-spike protein interaction. Mutagenesis (A529→I529) combined with Co-IP indicated that A529 was essential for the human TfR-spike protein interaction (Fig. 2*F*), which is consistent with sequence alignment in *SI Appendix*, Fig. S4*C*.

Physiological Occurrence of TfR-SARS-CoV-2 Interaction and TfR-Dependent SARS-CoV-2 Endocytosis. Our study found that TfR and the SARS-CoV-2 spike protein showed interaction in vitro. Thus, we investigated the physiological occurrence of the TfR-SARS-CoV-2 interaction. The Co-IP results revealed that the physiological interaction between TfR and SARS-CoV-2 spike protein occurred at the cell surface and during endocytosis (Fig. 3*A* and *SI Appendix*, Fig. S5). Electron microscopy further showed that TfR (traced by 5-nm gold colloid-labeled antibody) was bound to the spike protein (traced by 15-nm gold colloid-labeled antibody) of SARS-CoV-2 pseudovirus at cell surface and during endocytosis of HEK293/hACE2 and Baby Hamster Syrian Kidney-21 (BHK-21)/hTfR cells (Fig. 3*B* and *SI Appendix*, Fig. S6). Soluble TfR, Tf, anti-TfR antibody, and designed peptides (SL8 and QK8), which are predicted to block TfR-SARS-CoV-2 interaction by occupying TfR or blocking TfR-spike protein binding, were used to test their effects on SARS-CoV-2 infection using plaque assay and qRT-PCR assays. As expected, the results indicated that they inhibited viral infection in Calu-3 and Vero E6 cells (Fig. 3*C* and *SI Appendix*, Fig. S7). The concentrations required to inhibit 50% viral entry (EC_{50}) for soluble TfR, Tf, anti-TfR antibody, SL8, and QK8 were 92, 98, 35, 9,000, and 3,600 nM and 120, 132, 34, 1,100, and 3,500 nM, respectively (Fig. 3*C* and *SI Appendix*, Fig. S7). No cytotoxicity was observed, even at concentrations up to 1,000 nM. The time-of-addition assay showed that the anti-TfR antibody and SL8 efficiently functioned at the full-time and entry stages in the Calu-3 and Vero E6 cells (Fig. 3 *D* and *E* and *SI Appendix*, Fig. S8). More significant antiviral effect of anti-ACE2 antibody combined with anti-TfR antibody or SL8 at the entry stage (*SI Appendix*, Fig. S9). In addition, soluble TfR, Tf, anti-TfR antibody, and peptides significantly inhibited SARS-CoV-2-s pseudovirus entry in Calu-3 cells, rarely inhibited

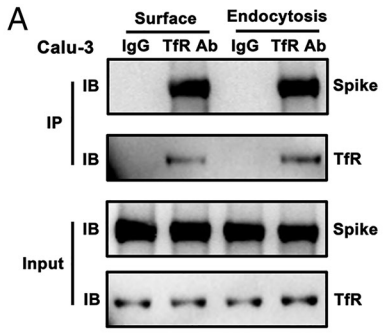

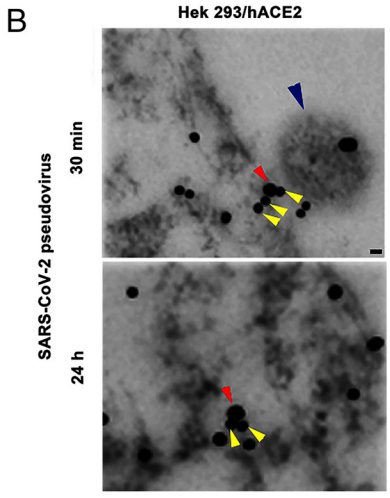

C

Test sample	The concentration to inhibit 50% viral entry (EC50)	
	Determined by plaque assay	Determined by quantitative qPCR
Soluble TfR	91.6 nM	120.2 nM
Tf	97.7 nM	132.0 nM
TfR antibody	34.8 nM	33.5 nM
SL8	9.0 μM	10.5 μM
QK8	3.6 μM	3.5 μM

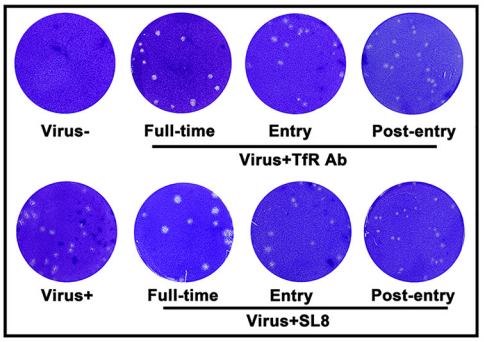

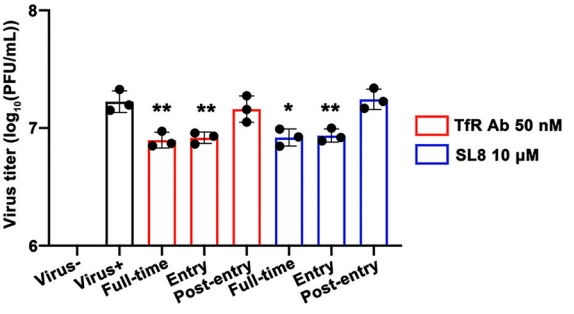

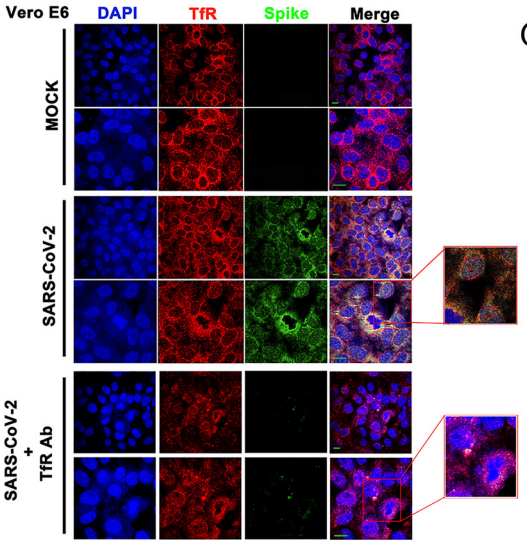

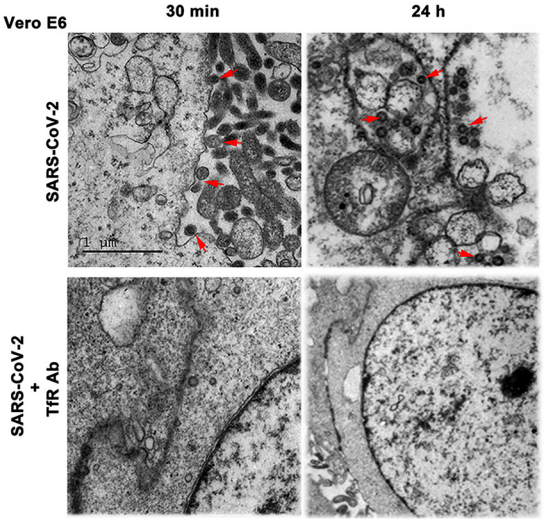

Fig. 3. Physiological occurrence of TfR-dependent SARS-CoV-2 endocytosis. (*A*) The Co-IP of spike with TfR during cell surface binding and endocytosis in human lung adenocarcinoma (Calu-3) cells infected with SARS-CoV-2. Images are representative of at least three independent experiments. (*B*) The co-localization of TfR (5-nm gold colloid, yellow arrow) and spike protein (15-nm gold colloid, red arrow) was observed during cell surface (*Top*) and endocytosis (*Bottom*) in SARS-CoV-2 pseudovirus-infected HEK293/hACE2 cells by immuno-electron microscopy. SARS-CoV-2 pseudovirus (blue arrow) is shown. (Scale bar, 8 nm.) Images are representative of at least three independent experiments. (*C*) Calu-3 cells were infected with SARS-CoV-2 (MOI, 0.05) and treated with different concentrations of TfR, Tf, anti-TfR antibody (TfR Ab), or different doses of inhibitory peptides (SL8 and QK8), and the concentration required to inhibit 50% viral entry was evaluated by the plaque assay and qRT-PCR, respectively. (*D*) Time-of-addition experiments (full-time, entry, and post-entry treatment) of the anti-TfR antibody (50 nM) or interference peptide SL8 (10 μM) were assayed in infected cells by plaque assay. (*E*) Corresponding quantification is shown at the *Bottom*. Data represent mean ± SD of three independent experiments, $*P < 0.05$, $**P < 0.01$ by the unpaired *t* test. (*F*) Vero E6 cells were infected with SARS-CoV-2 (MOI, 0.2) or uninfected (MOCK) for 2 h. Cells were labeled with both anti-TfR and anti-spike antibodies to observe TfR-spike protein co-localization. Cell nuclei were labeled by DAPI. White arrows indicate TfR-spike protein-positive structures on cell surface. Red arrows indicate endocytic TfR-spike protein-positive structures. (Scale bar, 10 μm.) Images are representative of at least three independent experiments. Vero E6 cells were infected with SARS-CoV-2 or treated with TfR Ab (500 nM) for 30 min and 24 h. TfR-dependent SARS-CoV-2 endocytosis was determined by electron microscopy (*G*). Virion (red arrows) is shown. Images are representative of at least three independent experiments. (Scale bar, 1 μm.) IP: immunoprecipitation; IB: immunoblotting.

SARS-CoV-1-s and VSV-g (vesicular stomatitis virus glycoprotein) pseudovirus entry (*SI Appendix*, Fig. S10). As illustrated in Fig. 3*F* and *SI Appendix*, Fig. S11, confocal microscopy showed that TfR was found at a high density on the surface of Vero E6 and Calu-3 cells. Following SARS-CoV-2 infection in cells, significant co-localizations of TfR and SARS-CoV-2 were observed at the cell surface and during endocytosis. In contrast, the anti-TfR antibody inhibited these co-localizations (Fig. 3*F* and *SI Appendix*, Fig. S11). To further investigate the SARS-CoV-2 internalization pathway, we performed electron microscopy of Vero E6 cells infected with SARS-CoV-2 for 30 min and 24 h. Viral particles were detected in both clathrin-coated pits and cytosol inside completely invaginated vesicles, while the anti-TfR antibody significantly inhibited the viral internalization (Fig. 3*G*). These results indicate that TfR can mediate SARS-CoV-2 endocytosis by directly interacting with the virus spike protein.

TfR-Mediated SARS-CoV-2 Infection Is ACE2 Independent. As TfR appears to mediate SARS-CoV-2 endocytosis (as shown above), we further investigated whether this ability is ACE2-dependent. ACE2 was deleted (ACE2 *KO*) in Calu-3 and Vero E6 cells, which were then infected with SARS-CoV-2 (*SI Appendix*, Fig. S12). Unexpectedly, ACE2 deficiency only partially inhibited SARS-CoV-2 infection (~40 to 50%) in those cells, suggesting that ACE2 is not the sole receptor mediating the viral infection (Fig. 4*A* and *SI Appendix*, Fig. S13). Notably, ACE2 knockout in combination with a TfR decoy (soluble TfR) further inhibited SARS-CoV-2 infection (Fig. 4*A* and *SI Appendix*, Fig. S13). Because TfR deficiency is lethal, we constructed TfR knock-down (TfR *KD*) cells to assess the function of TfR as an independent receptor. TfR *KD* inhibited viral infection by ~30% (ACE2 *KD* ~40%), whereas TfR overexpression (TfR *OE*) significantly increased viral infection by ~249% (ACE2 *OE* ~1,000%, Fig. 4*B* and *SI Appendix*, Figs. S14 and S15). Importantly, TfR *OE* and *KD* did not affect ACE2 expression (*SI Appendix*, Fig. S16). To further determine whether human TfR mediated SARS-CoV-2 infection, BHK-21 cells (*SI Appendix*, Fig. S17), which are non-permissive to SARS-CoV-2 entry (48), were overexpressed with human TfR and then infected with SARS-CoV-2 virus or pseudovirus. As illustrated in Fig. 4 *C* and *D* and S18, BHK-21 cells overexpressing human TfR and ACE2 were susceptible to SARS-CoV-2 infection and the Omicron had higher infectivity to overexpressed human TfR and ACE2 cells. These results, combined with direct TfR-SARS-CoV-2 interactions suggest that human TfR is a receptor mediating viral infection.

Mice Overexpressing hTfR Are Susceptible to SARS-CoV-2 Infection. Wild-type C57 mice are not susceptible to SARS-CoV-2 infection (49). To investigate the infection efficiency of SARS-CoV-2 to hTfR and hACE2, we constructed hTfR and hACE2 mouse models by transducing adenoviral vector (Ad5)-expressing human TfR (Ad5-hTfR) and Ad5-hACE2 intranasally into C57 mice as described in previous research (50) (*SI Appendix*, Fig. S19). Viral loads were detected in the lungs of Ad5-empty/hTfR/ACE2 mice infected with SARS-CoV-2 at 1-, 3-, and 5 d post-infection (dpi) (Fig. 4*E*). The viral load in the lung of Ad5-hACE2 and Ad5-hTfR mice maintained to a level that was still significantly higher than infected Ad5-empty mice from 3 to 5 dpi. Histopathological examination of lung sections indicated that hTfR/hACE2 mice had typical interstitial pneumonia, characterized by significant infiltration of large numbers of lymphocytes and macrophages, hyaloid membrane formation, and pulmonary consolidation (Fig. 4*F*). These results indicate that hTfR mice were susceptible to SARS-CoV-2 infection.

Anti-TfR Antibody Shows Significant Anti-SARS-CoV-2 Effects in Monkeys. The in vivo effects of anti-TfR antibody on SARS-CoV-2 infection were evaluated in a rhesus macaque model. Results showed that anti-TfR antibody inhibited SARS-CoV-2 replication and alleviated pneumonia in the monkeys (Fig. 5). At 7 dpi, the viral load in the lungs of the control group was ~10^8 copies/ng total RNA, whereas that in monkeys treated with the antibody (1.6 mg/kg intravenous injection administration at day 0, once per day) decreased to ~10^6 copies (Fig. 5*A*). Viral loads in respiratory epithelium of treated with anti-TfR antibody group were significantly inhibited at 3 to 7 dpi (Fig. 5*B*). The decrease in monkey body weight caused by viral infection was also inhibited by anti-TfR antibody (Fig. 5*C*). Radiographic pulmonary infiltration is a hallmark of COVID-19 in humans (51, 52). Here, radiographs taken on 0 and 5 dpi showed significantly less severe pulmonary infiltration in the macaques treated with anti-TfR antibody than in the saline control group (Fig. 5 *D*, *Top*). No significant pulmonary lesions were observed in the antibody-treated group while varying degrees of lung lesions at the gross pathological scale were observed in the control macaques (Fig. 5 *D*, *Bottom*). Histological evaluation showed severe (2/3) subpleural interstitial pneumonia and minimal (2/3) infiltration of neutrophils and congestion (2/3) in the vehicle-treated animals. However, only minimal (2/3) and moderate (1/3) subpleural interstitial pneumonia and minimal (1/3) infiltration of neutrophils were observed in the antibody-treated animals (Fig. 5 *E*, *Top*). IHC assay revealed that fewer viral antigens were detected in the lungs of macaques treated with anti-TfR antibodies compared with the saline control group (Fig. 5 *E*, *Bottom*). These results further confirmed the anti-SARS-CoV-2 effects of the anti-TfR antibody.

Discussion

SARS-CoV-2 has been detected in almost all human organs, including lungs, pharynx, heart, liver, brain, kidneys, and digestive system organs. However, ACE2 expression is deficient in many human tissues, such as brain (0%) and lungs (0.1%) (23). Single-cell sequencing data indicated the presence of SARS-CoV-2 RNAs in various immune cell types, including neutrophils, macrophages, plasma B cells, T and NK cells, but ACE2 is not expressed in these cells (29). All the studies suggest the presence of additional receptor for SARS-CoV-2 viral entry. Especially, ubiquitously expressed membrane receptors might be the candidates.

In the present study, we identified human TfR, a ubiquitously expressed membrane protein (41), as a receptor for SARS-CoV-2. TfR mediated SARS-CoV-2 infection by directly binding to the spike protein with high affinity and transporting the virus into the host cells. Interference with the TfR and SARS-CoV-2 interaction using soluble TfR, Tf, anti-TfR antibody, or designed peptides inhibited viral infection. Notably, the anti-TfR antibody showed promising antiviral effects in the rhesus macaque model. This work not only provided a potential antiviral strategy but also established an hTfR-expressing mouse model that could be used for studies on viral infection and drug screening.

Both TfR and Tf participate in essential cellular iron uptake. However, emerging evidence also suggests that many viruses use the host TfR to enter cells, which is thus a viral target for infection (41–43). Microbe infection causes iron deficiency and anemia (53) and both induce TfR expression (54). Our results showed that TfR expression was up-regulated by SARS-CoV-2 infection. Both the entry and infectivity of various viruses depend on the TfR trafficking pathway (42, 43, 55–66). Given that TfR is one of the most ubiquitously and highly expressed plasma membrane components, it is an attractive target for viruses to initiate host

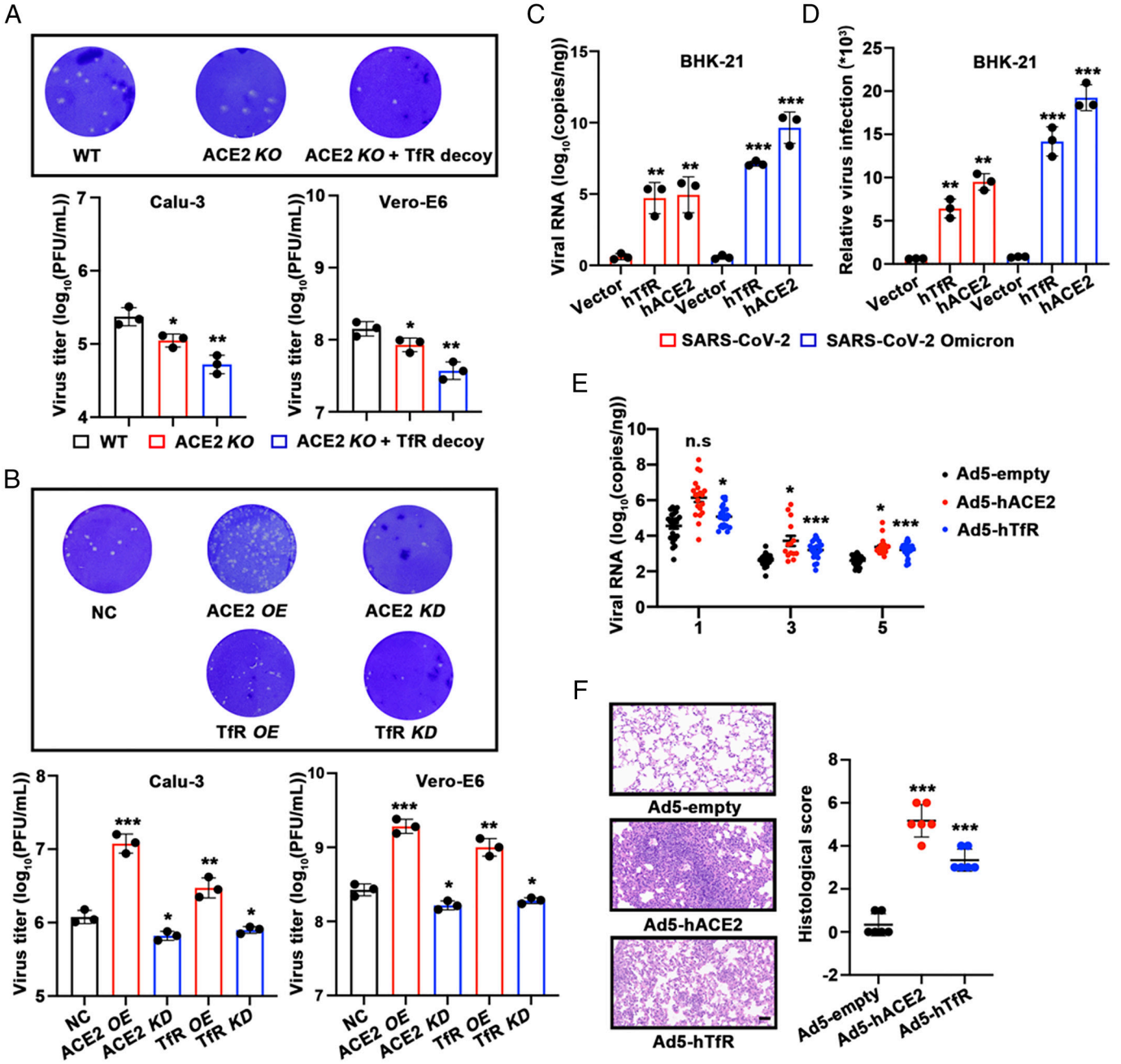

Fig. 4. TfR-mediated SARS-CoV-2 infection is ACE2 independent in both cellular and mouse models. (*A*) The inhibitory effect of ACE2-knockout (*KO*) and TfR decoy (TfR 200 nM) on virus infection (MOI, 0.2) was detected by plaque assay and quantified. (*B*) TfR overexpressed (*OE*) and knock-down (*KD*) Calu-3 and Vero E6 cells were infected with SARS-CoV-2 (MOI, 0.05), virus titer was detected by plaque assay. Data represent means ± SD of three independent experiments, **P*< 0.05, ***P*< 0.01, ****P* < 0.001 by one-way ANOVA with Dunnett's post-hoc test. Baby hamster Syrian kidney cells (BHK-21) were overexpressed with human TfR (hTfR) and ACE2 (hACE2), (*C*) viral RNA was quantified by RT-qPCR assay at 48 h post infection with SARS-CoV-2 original strain and Omicron variant (MOI, 0.4). (*D*) SARS-CoV-2 original strain and Omicron variant pseudovirus were inoculated and luciferase activity was measured. Data represent mean ± SD of three independent experiments, **P* < 0.05, ***P* < 0.01, ****P* < 0.001 by the unpaired *t* test. (*E*) Ad5-empty/hTfR/hACE2 transfected C57 mice were infected with SARS-CoV-2. Five lung lobes from all mouse groups were harvested for evaluation of viral loads at 1, 3, and 5 dpi, respectively. (*F*) Histopathological changes in mouse lung sections from all groups at 5 dpi were analyzed by hematoxylin and eosin (H&E) staining. Corresponding quantification is shown on the *Right*. (Scale bar, 50 μm.) Data represent mean ± SD (n = 6), **P* < 0.05, ****P* < 0.001 by the unpaired *t* test.

cell infection (42, 43). As illustrated in Fig. 1, high levels of TfR were found in mice's respiratory tracts, thus increasing the possibility that SARS-CoV-2 infection is predominantly transmitted among humans via the respiratory route.

Human TfR directly binds to the spike protein of SARS-CoV-2 with a binding affinity of K_D 2.95 nM, similar to the binding affinity range (31.59 to 4.67 nM) reported for ACE2 and SARS-CoV-2 and SARS-CoV in previous studies (16–20). However, mouse TfR showed no interaction with the spike protein. The physiological occurrence of TfR-SARS-CoV-2 interactions was further confirmed by Co-IP analysis. Co-IP analyses further confirmed the physiological interactions of TfR-SARS-CoV-2. TfR mutant experiments showed that A529 is essential for human TfR-spike protein interactions (Fig. 2*F*), and interestingly, the position is alanine in both humans and monkeys and is isoleucine in Syrian hamsters, mice, and rats, which may have contributed to the fact that spike does not bind to the TfR in Syrian hamsters, mice, and rats, making them highly tolerant to SARS-CoV-2 (*SI Appendix*, Fig. S4).

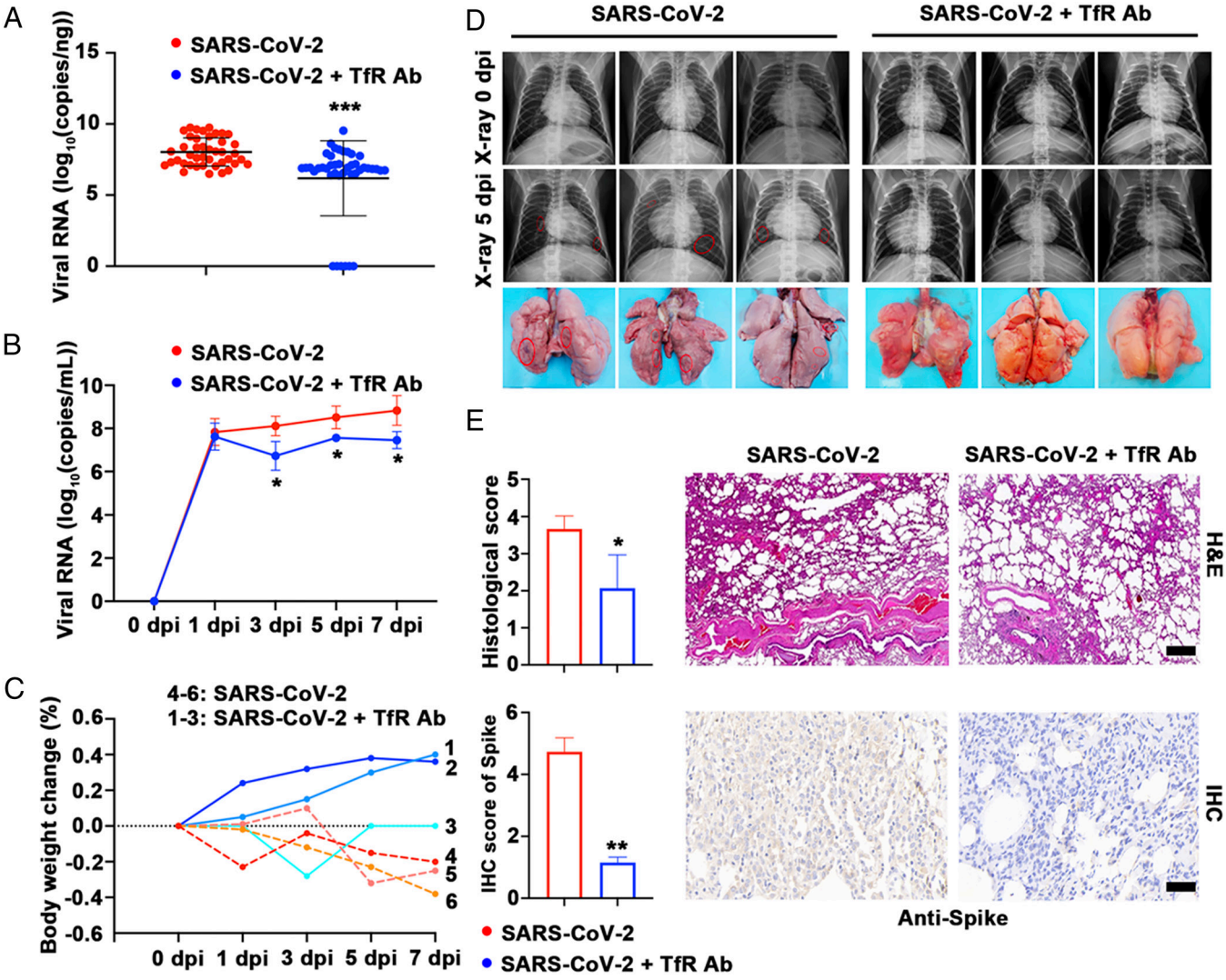

Fig. 5. Anti-TfR antibody shows significant anti-COVID-19 effects in the rhesus macaque model. Monkeys were randomly assigned to saline (SARS-CoV-2, n = 3) or anti-TfR antibody-treated groups (SARS-CoV-2 + 1.6 mg/kg monkey TfR Ab, n = 3) and inoculated with SARS-CoV-2 via intratracheal and intranasal administration. (*A*) All seven lung lobes from all monkey groups were harvested for evaluation of viral loads at 7 dpi. No viral RNA was detected in six of the forty-two samples, two of them from the lower left lobe of monkey 3 and the remaining from the middle and lower right lobe of monkey 1. (*B*) Viral loads in respiratory epithelium. (*C*) The body weight change of every monkey was recorded, 1 to 3: SARS-CoV-2 infected group, 4 and 5: SARS-CoV-2 and TfR Ab treatment group. (*D*, *Top*) Radiographs of each animal taken on 0 and 5 dpi are shown. (*D*, *Bottom*) The pulmonary infiltration area is marked with a red circle. Photographs of lung specimens of all monkey groups at 7 dpi are shown. (*E*) Histopathological changes and IHC in lung sections of all monkey groups at 7 dpi were analyzed by H&E staining and anti-spike antibody staining. Corresponding quantification is shown on the *Right*. (Scale bar, 50 μm.) Data represent mean ± SD (n = 3), $*P < 0.05$, $**P < 0.01$, $***P < 0.001$ by the unpaired *t* test (*A* and *E*) or two-way ANOVA and Fisher's least significant difference (LSD) tests (*B*).

Electron and confocal microscopy indicated that TfR mediated SARS-CoV-2 endocytosis. In virus-infected cells, the TfR-virus complex was found both on the cell surface and during endocytosis, while the anti-TfR antibody inhibited virus entry and infection. Notably, in Vero E6 cells, ACE2 knockout only partially blocked SARS-CoV-2 infection by 40 to 50%, whereas TfR knockdown significantly inhibited infection by ~30% and its overexpression increased infection by ~249%, indicating that TfR plays an important role in SARS-CoV-2 infection and its function is ACE2 independent. Furthermore, ACE2 knockout combined with a soluble TfR decoy further inhibits viral infection. Normal baby hamster Syrian kidney cells are known to be non-permissive to SARS-CoV-2 entry (48), but human TfR over-expression made it possible to be infected by the virus in the cells. In addition, hTfR mice were susceptible to SARS-CoV-2 infection (Fig. 4 *E* and *F*). Combined with TfR's ubiquitous and high expression in membranes, these data indicate that the TfR-spike protein complex acts as a machinery to mediate SARS-CoV-2 entry (*SI Appendix*, Fig. S20).

SARS-CoV-2 can enter host cells by two different pathways, either by fusion with the plasma membrane under activation of the cell surface protease TMPRSS2, or by endocytosis under activation of tissue proteases to fuse with the endonuclease/lysosomal membrane (67). Recent studies have shown that SARS-CoV-2 can use spike binding to TMEM106B (37) or NPC1 (38) to enter cells via endocytosis, TfR is likely to have a similar function to TMEM106B and NPC1. TMEM106B and NPC1 are located in endosomes, a few in the plasma membrane. In contrast, TfR is widely distributed in most cells and is abundantly expressed in both the plasma membrane and endosomes. Thus, TfR may be a "virus-binding ligand" that serves as an alternative infection pathway for viruses, facilitating viral entry into receptor- and protease-rich endosomes through endocytosis (*SI Appendix*, Fig. S20).

Iron overload is increasingly implicated as a contributor to the pathogenesis of COVID-19 (68–72). The high-affinity binding of the SARS-CoV-2 spike protein to TfR may interfere with the transport of iron by TfR-Tf to intracellular storage and utilization

(73), leading to iron overload (74). Iron overload plays a key role in influencing the susceptibility of cells to ferroptosis (75–77) and may further contribute to multi-organ damage and complications (78–80). As viral infection up-regulates the expression of TfR in mice and monkeys (Fig. 1 *C* and *D*), it may lead to increased susceptibility to viral infection (Fig. 4 *B*–*E*) and further lung damage (Figs. 4*F* and 5 *D* and *E*).

Notably, the soluble TfR, Tf, anti-TfR antibody, and peptides significantly blocked SARS-CoV-2 entry into Calu-3 and Vero E6 cells by interfering with TfR-SARS-CoV-2 interaction, anti-ACE2 antibody combined with anti-TfR antibody or SL8 has more significant antiviral effects, thus providing strategies for anti-SARS-CoV-2 treatment and for developing potent therapeutic agents. In vivo administration of the anti-TfR antibody significantly inhibited SARS-CoV-2 replication and alleviated pneumonia in the monkey model, showing promising antiviral potential. In addition, the designed peptides (SL8 and QK8), which interfere with TfR-SARS-CoV-2 interactions, showed efficacy in inhibiting virus entry, suggesting an approach to design small antiviral molecules.

Materials and Methods

Cells and Virus. Calu-3, Vero E6, and BHK-21 cell lines were cultured in DMEM (Gibco), 10% FBS at 37 °C in 5% CO_2. The original SARS-CoV-2 strain (GD108) and the SARS-CoV-2 Omicron variant (B.1.1.529) were propagated in the Vero E6 cells and amplified. For additional details, see *SI Appendix*.

SPR Analysis. BIAcore 2000 (GE) was used to analyze the interaction between TfR and the spike protein or spike protein RBD. The data were analyzed using BIAevaluation software, version 4.1 (GE). For additional details, see *SI Appendix*.

Electron Microscopy. Vero E6 and Calu-3 cells infected with SARS-CoV-2 for 30 min and 24 h were harvested by centrifugation at 500×*g* for 5 min. Cells were fixed with 2.5% glutaraldehyde without re-suspending the pellet at 4 °C overnight. Sections were made and stained with 2% uranium acetate and lead citrate after cells were embedded in epoxy resin and ultrathin. Slides were imaged under an electron microscope (JEM 1400Plus).

Immuno-electron microscopy was used to observe the co-localization of TfR and the spike protein in HEK293/hACE2 (OEC001, Sino Biological) and BHK-21/hTfR cells infected with SARS-CoV-2-s pseudovirus (PSV001, Sino Biological), with the sections prepared as described above. Sections were incubated with corresponding primary antibodies (mouse anti-human TfR antibody (11020-MM04, Sino Biological); rabbit anti-SARS-CoV-2-spike antibody (40150T62-COV2, Sino Biological) for 2 h at room temperature overnight after blocking with 1% BSA for 30 min. Subsequently, the sections were washed with PBS and incubated with 1% BSA for another 30 min. Secondary antibodies (5-nm gold-colloid labeled goat anti-mouse IgG (G7527, Sigma-Aldrich) and 15-nm gold-colloid labeled goat anti-rabbit IgG (ab27236, Abcam) were used to determine the localization of target proteins. Slides were imaged under an electron microscope as described above.

Antiviral Evaluation. To evaluate the antiviral efficacy of TfR (11020-H07H, Sino Biological), Tf (T4382, Sigma), anti-TfR antibody (self-produced), and interference peptides, the Calu-3 and Vero E6 cells were pretreated with different doses of these samples for 1 h, and the virus (multiplicity of infection, MOI, 0.05) was subsequently added to allow infection for 1 h. The virus-protein mixture was removed, and cells were further cultured with fresh protein-containing medium. At 48 h, the Intracellular viral RNA was extracted by using TRIzol reagent (15596018CN, Invitrogen) as recommended by the manufacturer, the cell supernatant was collected and lysed in lysis buffer (15596018, Thermo) for qRT-PCR, as described previously (81, 82). The qRT-PCR protocols were performed as described above (83). The supernatants from infected cells as above were added to fresh Vero E6 cells and incubated for 2 h at 37 °C and discarded. Cells were overlaid with 2 mL of a mix of 4% agarose and 2X DMEM medium with 4% FBS and incubated at 37 °C for 2 d, followed by fixation with 4% formaldehyde. After overlay removal, cells were stained with 0.5% crystal violet, washed, and dried. Plaques were counted for the determination of viral titer. The primer and probe sequences were listed as follows:

SARS-CoV-2-Forward: 5′-GGGGAACTTCTCCTGCTAGAAT-3′
SARS-CoV-2-Reverse: 5′-CAGACATTTTGCTCTCAAGCTG-3′
SARS-CoV-2-Probe: 5′-FAM-TTGCTGCTGCTTGACAGATT-TAMRA-3′

CRISPR/Cas9-Mediated ACE2 Knockout. We used the CRISPR/Cas9 system to establish stable ACE2 knockout in Calu-3 and Vero E6 cells. We designed guide RNA (gRNA) sequences (gRNA1: TGCTGCTCAGTCCACCATTG for monkey ACE2, gRNA2: ACAGTTTAGACTACAATGAG for human ACE2) targeting the ACE2 locus and cloned into the lentiCRISPRv2 puro plasmid (98290, Addgene plasmid). Constructed plasmids were co-transfected into HEK-293T cells with packaging plasmids pCMV-dR8.91 (VT1441, YouBio) and pMD2.G (VT1443, YouBio) at a ratio of 10:5:2. The culture medium was collected and filtered. The resulting supernatant containing lentiviral particles was used to infect the Vero E6 and Calu-3 cells. After 24 h of puromycin screening, a single-cell culture was established using the limiting dilution method. The ACE2-null clones were screened by DNA and cDNA sequencing, western blotting, and flow cytometry.

TfR and ACE2 Overexpression and Knockdown. The coding region of the green monkey TfR (GenBank: 103242011), green monkey ACE2 (GenBank: 103231639), human TfR (GenBank: 7037), and ACE2 (GenBank: 59272) were synthesized and cloned into the pLVX-Puro lentiviral plasmids (Clontech, USA) as per our previous study (84). The oligonucleotides of the shRNA sequence targeting the green monkey TfR, green monkey ACE2, human TfR, and human ACE2 were synthesized by Sangon Biotech and inserted into the BamHI and EcoRI sites of the RNAi-Ready pSIREN-RetroQ retroviral vector (Clontech), as described previously (84). The lentiviral vector for overexpression and retroviral vector for knockdown were transfected into Calu-3 and Vero E6 cells to construct overexpression or knockdown cells, respectively. BHK-21 cells (were overexpressed with human TfR and ACE2) using the same method described above. SARS-CoV-2s and SARS-CoV-2s Omicron (PSV017, Sino Biological) pseudovirus were inoculated and luciferase activity was measured as described above. Virus titers were also measured in human TfR and ACE2 overexpressed BHK-21 cells by RT-qPCR assay at 48 h post infection with SARS-CoV-2 (MOI, 0.4) as described above. The shRNA sequences were listed as follows:

Human TfR shRNA: 5′-GAACTTCAAGGTTTCTGCCAGCTT-3′
Human ACE2 shRNA: 5′-GCACTTTGTCAAGCAGCTATT-3′
Green monkey TfR shRNA: 5′-GGATCTATAGTGATTGTCATT-3′
Green monkey ACE2 shRNA: 5′-GAGGAGACTATGAAGTAAATT-3′

Human TfR-Expressing Adenoviral Vector Construction and Transduction in Mice. The adenoviral vector Ad5 (pAD100010-OE, Vigene Biosciences, China) expressing hTfR and hACE2 was constructed as described in other studies (50). Mice were anesthetized and transduced intranasally with 3×10^8 PFU of Ad5-empty vector, Ad5-hTfR, and Ad5-hACE2 in DMEM (Gibco Laboratories). Mice were infected intranasally with 10^6 $TCID_{50}$ SARS-CoV-2 after 4 d of transduction. The mice were killed and dissected at 1-, 3-, and 5 d post-infection (dpi), respectively, to collect different tissues for the screening of virus titer and histopathological changes.

In Vivo Anti-SARS-CoV-2 Assays of Anti-TfR Antibody in Monkeys. A rhesus macaque model of SARS-CoV-2 infection was used to evaluate the effects of the anti-TfR antibody (self-produced) on SARS-CoV-2 infection. Rhesus macaques (males, 8 y old, ~8 to 10 kg) were randomly assigned to two groups, i.e., saline group (n = 3) and anti-TfR antibody-treated group (1.6 mg/kg; n = 3) inoculated with SARS-CoV-2 (10^6 $TCID_{50}$) by intratracheal and intranasal administration. Animals were daily checked for clinical signs after viral inoculation. The animals were then anesthetized with ketamine for experimental procedures, including body temperature and weight monitoring, sample collection, chest radiography, and necropsies at the indicated stages. For details regarding animals and ethics statement, see *SI Appendix*.

Statistical Analysis The data obtained from independent experiments were presented as the mean ± SD. All statistical analyses were two-tailed and with 95% CI. The Kolmogorov–Smirnov test (K–S test) was used in the analysis of normal distribution, and data were then analyzed using one-way ANOVA, or two-way ANOVA in case of measuring the effects of two factors simultaneously, with

post hoc Dunnett or Bonferroni adjustment for P values. If only two groups were compared, the unpaired t test was applied. Data were analyzed using Prism 6 (GraphPad Software) and SPSS (SPSS Inc.). Differences were considered significant at $P < 0.05$.

Data, Materials, and Software Availability. All study data are included in the article and/or *SI Appendix*. All the files are available at Figshare (https://doi.org/10.6084/m9.figshare.25158179.v1) (85).

ACKNOWLEDGMENTS. This work was supported by the Ministry of Science and Technology of China (2018YFA0801403, R.L. and 2022YFC2105003, Z.D.), NSF of China (31930015, R.L., 32100907, 32371162, X.T., and U2002219, Z.D.), Chinese Academy of Sciences (KFJ-BRP-008 and SAJC202103, R.L.), Excellent Young Scientists Foundation of Shandong Province (ZR2023YQ025, X.T.), Yunnan Province (202003AD150008, R.L., 202202AA100002 and 202301AS070074, X.T.), Kunming Science and Technology Bureau (2022SCP007, R.L.) and New Cornerstone Investigator Program from Shenzhen New Cornerstone Science Foundation.

Author affiliations: [a]Engineering Laboratory of Peptides of Chinese Academy of Sciences, Key Laboratory of Bioactive Peptides of Yunnan Province, Kunming Institute of Zoology-Chinese University of Hong Kong Joint Laboratory of Bioresources and Molecular Research in Common Diseases, National Resource Center for Non-Human Primates, National Research Facility for Phenotypic & Genetic Analysis of Model Animals (Primate Facility), and Sino-African Joint Research Center, New Cornerstone Science Laboratory, Kunming Institute of Zoology, The Chinese Academy of Sciences, Kunming 650201, China; [b]Kunming College of Life Science, University of Chinese Academy of Sciences, Beijing 100049, China; [c]School of Basic Medicine, Qingdao University, Qingdao 266071, China; [d]Institute of Medical Biology, Chinese Academy of Medical Sciences, Kunming 650118, China; [e]Laboratory of Animal Tumor Models, Frontiers Science Center for Disease-Related Molecular Network, State Key Laboratory of Biotherapy and Cancer Center, National Clinical Research Center for Geriatrics, West China Hospital, Sichuan University, Chengdu 610041, China; and [f]Kunming Institute of Botany, Chinese Academy of Sciences, Kunming 650204, China

1. V. J. Munster, M. Koopmans, N. van Doremalen, D. van Riel, E. de Wit, A novel coronavirus emerging in China–Key questions for impact assessment. *N. Engl. J. Med.* **382**, 692–694 (2020).
2. F. Zhou *et al.*, Clinical course and risk factors for mortality of adult inpatients with COVID-19 in Wuhan, China: A retrospective cohort study. *Lancet* **395**, 1054–1062 (2020).
3. P. Zhou *et al.*, A pneumonia outbreak associated with a new coronavirus of probable bat origin. *Nature* **579**, 270 (2020).
4. N. Zhu *et al.*, A novel coronavirus from patients with pneumonia in China, 2019. *N. Engl. J. Med.* **382**, 727–733 (2020).
5. X. Yang, Y. Yu, J. Xu, Clinical course and outcomes of critically ill patients with SARS-CoV-2 pneumonia in Wuhan, China: A single-centred, retrospective, observational study (vol 17, pg 534, 2020). *Lancet Resp. Med.* **8**, E26 (2020).
6. Z. Xu, L. Shi, Y. Wang, Pathological findings of COVID-19 associated with acute respiratory distress syndrome (vol 8, pg 420, 2020). *Lancet Resp. Med.* **8**, E26 (2020).
7. R. Lu *et al.*, Genomic characterisation and epidemiology of 2019 novel coronavirus: Implications for virus origins and receptor binding. *Lancet* **395**, 565–574 (2020).
8. W. J. Guan *et al.*, Clinical characteristics of coronavirus disease 2019 in China. *N. Engl. J. Med.* **382**, 1708–1720 (2020).
9. Coronaviridae Study Group of the International Committee on Taxonomy of Viruses, The species Severe acute respiratory syndrome-related coronavirus: Classifying 2019-nCoV and naming it SARS-CoV-2. *Nat. Microbiol.* **5**, 536–544 (2020).
10. T. M. V. Strabelli, D. E. Uip, COVID-19 and the heart. *Arq. Bras. Cardiol.* **114**, 598–600 (2020).
11. J. Zhang, B. Xie, K. Hashimoto, Current status of potential therapeutic candidates for the COVID-19 crisis. *Brain Behav. Immun.* **87**, 59–73 (2020), 10.1016/j.bbi.2020.04.046.
12. Y. Imai *et al.*, Angiotensin-converting enzyme 2 protects from severe acute lung failure. *Nature* **436**, 112–116 (2005).
13. K. Kuba *et al.*, A crucial role of angiotensin converting enzyme 2 (ACE2) in SARS coronavirus–induced lung injury. *Nat. Med.* **11**, 875–879 (2005).
14. C. Drosten *et al.*, Identification of a novel coronavirus in patients with severe acute respiratory syndrome. *N. Engl. J. Med.* **348**, 1967–1976 (2003).
15. J. F. Chan *et al.*, Genomic characterization of the 2019 novel human-pathogenic coronavirus isolated from a patient with atypical pneumonia after visiting Wuhan. *Emerg. Microbes Infect.* **9**, 221–236 (2020).
16. A. C. Walls *et al.*, Structure, function, and antigenicity of the SARS-CoV-2 spike glycoprotein. *Cell* **181**, 281–292.e286 (2020).
17. Y. Wan, J. Shang, R. Graham, R. S. Baric, F. Li, Receptor recognition by the novel coronavirus from wuhan: An analysis based on decade-long structural studies of SARS coronavirus. *J. Virol.* **94** (2020).
18. D. Wrapp *et al.*, Cryo-EM structure of the 2019-nCoV spike in the prefusion conformation. *Science* **367**, 1260–1263 (2020).
19. V. Monteil *et al.*, Inhibition of SARS-CoV-2 infections in engineered human tissues using clinical-grade soluble human ACE2. *Cell* **181**, 905–913.e7 (2020), 10.1016/j.cell.2020.04.004.
20. J. Lan *et al.*, Structure of the SARS-CoV-2 spike receptor-binding domain bound to the ACE2 receptor. *Nature* **581**, 215–220 (2020), 10.1038/s41586-020-2180-5.
21. M. Hoffmann *et al.*, SARS-CoV-2 cell entry depends on ACE2 and TMPRSS2 and is blocked by a clinically proven protease inhibitor. *Cell* **181**, 271–280.e278 (2020).
22. L. Zou *et al.*, SARS-CoV-2 viral load in upper respiratory specimens of infected patients. *N. Engl. J. Med.* **382**, 1177–1179 (2020).
23. M. M. Lamers *et al.*, SARS-CoV-2 productively infects human gut enterocytes. *Science* **369**, 50–54 (2020).
24. V. G. Puelles *et al.*, Multiorgan and renal tropism of SARS-CoV-2. *N. Engl. J. Med.* **383**, 590–592 (2020).
25. L. Lin *et al.*, Gastrointestinal symptoms of 95 cases with SARS-CoV-2 infection. *Gut* **69**, 997–1001 (2020).
26. S. Lukassen *et al.*, SARS-CoV-2 receptor ACE2 and TMPRSS2 are primarily expressed in bronchial transient secretory cells. *EMBO J.* **39**, e105114 (2020).
27. W. Sungnak *et al.*, SARS-CoV-2 entry factors are highly expressed in nasal epithelial cells together with innate immune genes. *Nat. Med.* **26**, 681–687 (2020).
28. X. P. Han *et al.*, Construction of a human cell landscape at single-cell level. *Nature* **581**, 303 (2020).
29. X. Ren *et al.*, COVID-19 immune features revealed by a large-scale single cell transcriptome atlas. *Cell* **184**, 1895–1913.e19 (2021), 10.1016/j.cell.2021.01.053.
30. L. Cantuti-Castelvetri *et al.*, Neuropilin-1 facilitates SARS-CoV-2 cell entry and infectivity. *Science* **370**, 856–860 (2020), 10.1126/science.abd2985.
31. S. Wang *et al.*, AXL is a candidate receptor for SARS-CoV-2 that promotes infection of pulmonary and bronchial epithelial cells. *Cell Res.* **31**, 126–140 (2021), 10.1038/s41422-020-00460-y.
32. N. S. Brunetti *et al.*, SARS-CoV-2 uses CD4 to infect T helper lymphocytes.*Elife* **12**, e84790 (2023). 10.7554/eLife.84790.
33. K. Wang *et al.*, CD147-spike protein is a novel route for SARS-CoV-2 infection to host cells. *Signal. Transduct. Target. Ther.* **5**, 283 (2020).
34. Y. Q. Gu *et al.*, Receptome profiling identifies KREMEN1 and ASGR1 as alternative functional receptors of SARS-CoV-2. *Cell Res.* **32**, 24–37 (2022).
35. Q. Zhang *et al.*, Heparan sulfate assists SARS-CoV-2 in cell entry and can be targeted by approved drugs in vitro. *Cell Discov.* **6**, 80 (2020).
36. L. Nguyen *et al.*, Sialic acid-containing glycolipids mediate binding and viral entry of SARS-CoV-2. *Nat. Chem. Biol.* **18**, 81–90 (2022).
37. J. Baggen *et al.*, TMEM106B is a receptor mediating ACE2-independent SARS-CoV-2 cell entry. *Cell* **186**, 3427–3442.e3422 (2023).
38. I. García-Dorival *et al.*, Identification of Niemann-Pick C1 protein as a potential novel SARS-CoV-2 intracellular target. *Antiviral Res.* **194**, 105167 (2021).
39. J. Song *et al.*, LRRC15 is an inhibitory receptor blocking SARS-CoV-2 spike-mediated entry in trans. bioRxiv [Preprint] (2021). https://doi.org/10.1101/2021.11.23.469714 (Accessed 23 November 2021).
40. J. Shang *et al.*, Structural basis of receptor recognition by SARS-CoV-2. *Nature* **581**, 221–224 (2020).
41. M. Wessling-Resnick, Crossing the iron gate: Why and how transferrin receptors mediate viral entry. *Annu. Rev. Nutr.* **38**, 431–458 (2018).
42. J. S. L. Parker, W. J. Murphy, D. Wang, S. J. O'Brien, C. R. Parrish, Canine and feline parvoviruses can use human or feline transferrin receptors to bind, enter, and infect cells. *J. Virol.* **75**, 3896–3902 (2001).
43. H. Koppensteiner *et al.*, Lentiviral Nef suppresses iron uptake in a strain specific manner through inhibition of Transferrin endocytosis. *Retrovirology* **11**, 1 (2014).
44. J. Shang *et al.*, Structural basis of receptor recognition by SARS-CoV-2. *Nature* **581**, 221–224 (2020), 10.1038/s41586-020-2179-y.
45. Y. Chen, Y. Guo, Y. Pan, Z. J. Zhao, Structure analysis of the receptor binding of 2019-nCoV. *Biochem. Biophys. Res. Commun.* **525**, 135–140 (2020), 10.1016/j.bbrc.2020.02.071.
46. C. M. Lawrence *et al.*, Crystal structure of the ectodomain of human transferrin receptor. *Science* **286**, 779–782 (1999).
47. Q. Wang *et al.*, Structural and functional basis of SARS-CoV-2 entry by using human ACE2. *Cell* **181**, 894–904.e9 (2020), 10.1016/j.cell.2020.03.045.
48. C. Conceicao *et al.*, The SARS-CoV-2 Spike protein has a broad tropism for mammalian ACE2 proteins. *PLoS Biol.* **18**, e3001016 (2020).
49. T. Pan *et al.*, Infection of wild-type mice by SARS-CoV-2 B.1.351 variant indicates a possible novel cross-species transmission route. *Signal. Transduct. Target. Ther.* **6**, 420 (2021).
50. J. Sun *et al.*, Generation of a broadly useful model for COVID-19 pathogenesis, vaccination, and treatment. *Cell* **182**, 734–743.e735 (2020).
51. A. E. Kaufman *et al.*, Review of radiographic findings in COVID-19. *World J. Radiol.* **12**, 142–155 (2020).
52. A. Pormohammad *et al.*, Clinical characteristics, laboratory findings, radiographic signs and outcomes of 61,742 patients with confirmed COVID-19 infection: A systematic review and meta-analysis. *Microb. Pathog.* **147**, 104390 (2020).
53. M. Nairz, G. Weiss, Iron in infection and immunity. *Mol. Aspects Med.* **75**, 100864 (2020), 10.1016/j.mam.2020.100864.
54. F. Bermejo, S. Garcia-Lopez, A guide to diagnosis of iron deficiency and iron deficiency anemia in digestive diseases. *World J. Gastroenterol.* **15**, 4638–4643 (2009).
55. G. S. Park, S. M. Best, M. E. Bloom, Two mink parvoviruses use different cellular receptors for entry into CRFK cells. *Virology* **340**, 1–9 (2005).
56. L. M. Palermo, K. Hueffer, C. R. Parrish, Residues in the apical domain of the feline and canine transferrin receptors control host-specific binding and cell infection of canine and feline parvoviruses. *J. Virol.* **77**, 8915–8923 (2003).
57. L. B. Goodman *et al.*, Binding site on the transferrin receptor for the parvovirus capsid and effects of altered affinity on cell uptake and infection. *J. Virol.* **84**, 4969–4978 (2010).
58. S. R. Radoshitzky *et al.*, Transferrin receptor 1 is a cellular receptor for New World haemorrhagic fever arenaviruses. *Nature* **446**, 92–96 (2007).
59. N. Sarute, S. R. Ross, New World arenavirus biology. *Annu. Rev. Virol.* **4**, 141–158 (2017).
60. S. R. Ross, J. J. Schofield, C. J. Farr, M. Bucan, Mouse transferrin receptor 1 is the cell entry receptor for mouse mammary tumor virus. *Proc. Natl. Acad. Sci. U.S.A.* **99**, 12386–12390 (2002).
61. E. Wang *et al.*, Mouse mammary tumor virus uses mouse but not human transferrin receptor 1 to reach a low pH compartment and infect cells. *Virology* **381**, 230–240 (2008).
62. J. L. Foster, J. V. Garcia, HIV-1 Nef: At the crossroads. *Retrovirology* **5**, 84 (2008).
63. H. Drakesmith *et al.*, HIV-1 Nef down-regulates the hemochromatosis protein HFE, manipulating cellular iron homeostasis. *Proc. Natl. Acad. Sci. U.S.A.* **102**, 11017–11022 (2005).

64. D. N. Martin, S. L. Uprichard, Identification of transferrin receptor 1 as a hepatitis C virus entry factor. *Proc. Natl. Acad. Sci. U.S.A.* **110**, 10777–10782 (2013).
65. H. Xia, B. Anderson, Q. Mao, B. L. Davidson, Recombinant human adenovirus: Targeting to the human transferrin receptor improves gene transfer to brain microcapillary endothelium. *J. Virol.* **74**, 11359–11366 (2000).
66. P. P. Rose *et al.*, Natural resistance-associated macrophage protein is a cellular receptor for sindbis virus in both insect and mammalian hosts. *Cell Host Microbe* **10**, 97–104 (2011).
67. C. B. Jackson, M. Farzan, B. Chen, H. Choe, Mechanisms of SARS-CoV-2 entry into cells. *Nat. Rev. Mol. Cell Biol.* **23**, 3–20 (2022).
68. H. M. Habib, S. Ibrahim, A. Zaim, W. H. Ibrahim, The role of iron in the pathogenesis of COVID-19 and possible treatment with lactoferrin and other iron chelators. *Biomed. Pharmacother.* **136**, 111228 (2021).
69. Y. Gupta *et al.*, Iron dysregulation in COVID-19 and reciprocal evolution of SARS-CoV-2: Natura nihil frustra facit. *J. Cell Biochem.* **123**, 601–619 (2022).
70. S. A. G. Naidu, R. A. Clemens, A. S. Naidu, SARS-CoV-2 infection dysregulates host iron (Fe)-redox homeostasis (Fe-R-H): Role of Fe-redox regulators, ferroptosis inhibitors, anticoagulants, and iron-chelators in COVID-19 control. *J. Diet Suppl.* **20**, 312–371 (2022), 10.1080/19390211.2022.2075072.
71. E. Campione *et al.*, Lactoferrin against SARS-CoV-2: In vitro and in silico evidences. *Front Pharmacol.* **12**, 666600 (2021).
72. A. Cavezzi, E. Troiani, S. Corrao, COVID-19: Hemoglobin, iron, and hypoxia beyond inflammation. A narrative review. *Clin. Pract.* **10**, 1271 (2020).
73. H. Kawabata, Transferrin and transferrin receptors update. *Free Radic. Biol. Med.* **133**, 46–54 (2019).
74. A. M. Fratta Pasini, C. Stranieri, D. Girelli, F. Busti, L. Cominacini, Is ferroptosis a key component of the process leading to multiorgan damage in COVID-19? *Antioxidants (Basel)* **10**, 1677 (2021).
75. S. J. Dixon *et al.*, Ferroptosis: An iron-dependent form of nonapoptotic cell death. *Cell* **149**, 1060–1072 (2012).
76. B. R. Stockwell *et al.*, Ferroptosis: A regulated cell death nexus linking metabolism, redox biology, and disease. *Cell* **171**, 273–285 (2017).
77. E. Park, S. W. Chung, ROS-mediated autophagy increases intracellular iron levels and ferroptosis by ferritin and transferrin receptor regulation. *Cell Death Dis.* **10**, 822 (2019).
78. S. V. Torti, F. M. Torti, Iron and cancer: More ore to be mined. *Nat. Rev. Cancer* **13**, 342–355 (2013).
79. K. Miyanishi, S. Tanaka, H. Sakamoto, J. Kato, The role of iron in hepatic inflammation and hepatocellular carcinoma. *Free Radic. Biol. Med.* **133**, 200–205 (2019).
80. E. Campione *et al.*, Lactoferrin as protective natural barrier of respiratory and intestinal mucosa against coronavirus infection and inflammation. *Int. J. Mol. Sci.* **21**, 4903 (2020).
81. M. Wang *et al.*, Remdesivir and chloroquine effectively inhibit the recently emerged novel coronavirus (2019-nCoV) in vitro. *Cell Res.* **30**, 269–271 (2020).
82. S. De Meyer *et al.*, Lack of antiviral activity of darunavir against SARS-CoV-2. *Int J. Infect Dis.* **97**, 7–10 (2020).
83. S. Lu *et al.*, Comparison of nonhuman primates identified the suitable model for COVID-19. *Signal. Transduct. Target. Ther.* **5**, 157 (2020).
84. X. Tang *et al.*, Transferrin plays a central role in coagulation balance by interacting with clotting factors. *Cell Res.* **30**, 119–132 (2020).
85. Z. Liao *et al.*, Human transferrin receptor can mediate SARS-CoV-2 infection. Figshare. https://doi.org/10.6084/m9.figshare.25158179.v1. Deposited 7 February 2024.